# Reconstruction of attosecond X-ray temporal fields with machine learning

Paris Franz

**Abstract**—Attosecond X-ray pulses at free-electron lasers are experimentally measured using the angular streaking technique, which maps the temporal information of X-ray pulses to a 2D photoelectron momentum spectrum. Here we investigate using machine learning denoise the measured 2D spectra, and to efficiently and accurately reconstruct the X-ray temporal fields from the single-shot 2D spectra. Qualitative and quantitative comparison of the machine learning methods to the standard are shown.

**Index Terms**—Image Processing, Reconstruction

## 1 Introduction

X-ray Free Electron Lasers (XFELs) are extending their capabilities to the attosecond regime. At the Linac Coherent Light Source (LCLS) at SLAC National Accelerator Lab, the XLEAP project has recently developed several attosecond soft x-ray modes. These sub-femtosecond modes are too short to be resolved using standard beamline measurements at LCLS, and instead are experimentally characterized using an angular streaking technique [1].

The angular streaking measurement uses a coaxial velocity map imaging spectrometer (cVMI) to measure the time-profile of attosecond XFEL pulses. The cVMI spectrometer encodes the single-shot temporal information of the electric field of an X-ray pulse into a 2D photoelectron momentum distribution. The X-ray pulse time-profile must be extracted from this 2D image via a reconstruction method.

This project's goal is to take an experimental angular streaking image and retrieve the temporal profile of the X-ray pulse.

## 2 Related Work

The angular streaking measurement is regularly used at XFELs to characterize the X-ray temporal pulse profiles [1], [2], [3]. At LCLS, to reconstruct X-ray pulses from this measurement, the photoelectron spectra are preprocessed to removed noise and a forward model is used to solve for the maximum a posterior (MAP) solution 1. This solving takes place within an outer loop over several values of unknown variable, Up, in the image formation model.

This method is shown in Fig. 1 and the image formation model is described in detail in [1]. This MAP fitting method has been used successfully; however, the current reconstruction procedure is relatively slow compared to the 120 Hz data acquisition rate at LCLS, with reconstruction of a single shot taking 10 minutes. Additionally, the experimentally measured 2D photoelectron spectrum require background and noise removal to be applied prior to fitting. Altogether, these challenges prohibit the online reconstruction of the temporal X-ray field.

## 3 Proposed Method

We use machine learning to investigate denoising the measured data, and reconstructing simulated angular streaking data.

### 3.1 Denoise with DnCNN

We use a modified DnCNN [4] to remove background from experimental 2D photoelectron spectra images, see Fig. 2. We use 3 hidden layers with 124 hidden channels for the DnCNN. We train the network on 446 pairs of noisy experimental photoelectron spectra and clean photoelectron spectra. The clean spectra are generated from the measured X-ray photon spectra and the image formation model. The experimental data used for this denoising task is a special subset of the data that does not depend on phase information, allowing us to use the image formation model with only the X-ray intensity spectra and not the full complex field.

We compare the denoised photoelectron spectra images with the standard background-subtraction method [2], where a background is separated from the experimental raw image using a physics-based model.

### 3.2 Reconstruction with a NN

We implement a neural network with the goal of quickly and accurately reconstructing X-ray temporal fields from angular streaking data.

We generate a training set of size 9500, a validation set of size 200, and a test set of size 300 using the image formation model described in [1]. The input to the network is the 2D photoelectron spectrum (size 52x52) and X-ray spectrum (size 1x300), and the output is the complex X-ray temporal field (size 1x600). NN has 5 layers, where the input layer size is 3004, the 2nd layer size is 2048, and otherwise the hidden layer size is 1024, as shown in Fig. 3. For optimization, we use ADAM with a learning rate of 1e-6.

- *P. Franz is with the Department of Applied Physics, Stanford University, Stanford, CA, 94305, USA.*
  *E-mail: franzpl@stanford.edu*

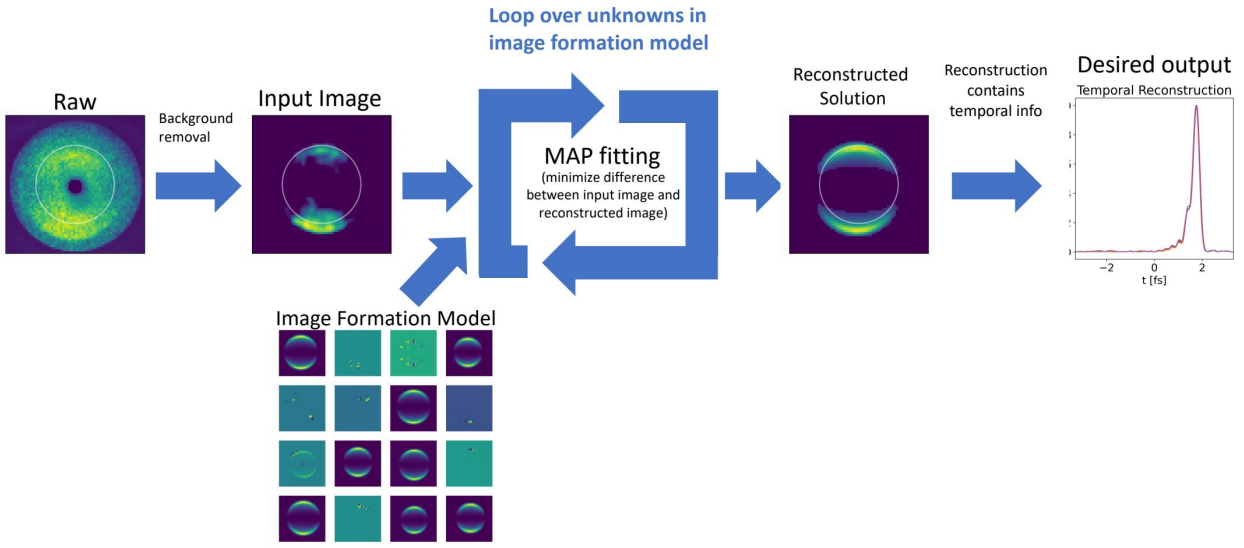


Fig. 1. Scheme of the standard MAP reconstruction algorithm. The raw measured 2D photoelectron spectrum undergoes background removal, and is input into a MAP solver. This solving takes place within an outer loop over several values of unknown variable Up in the image formation model. The reconstructed solution gives the desired temporal information of the X-ray field.

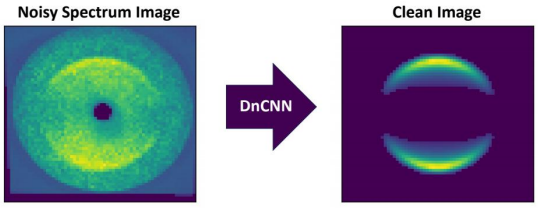


Fig. 2. Scheme of denoising the experimental images using DnCNN. The inputs are the 2D photoelectron spectra, and the output is the cleaned photoelectron spectra.

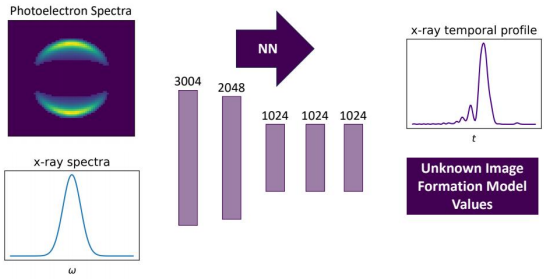


Fig. 3. Scheme of the NN. The inputs are the 2D photoelectron spectra and the 1D X-ray spectra. The outputs are the 1D X-ray temporal field and the unknown variable Up.

We implement this network using pytorch [5]. The loss function is the weighted sum of the L2 norm of the X-ray temporal field, the L2 norm of the FFT of the normalized X-ray temporal field, and the L2 norm of the unknown variable Up.

The original algorithm planned for this project involved several CNN layers at the start of the network, before flattening the output to input into linear layers. However, during the course of this project, we were unable to determine the correct hyperparameters for training such a network. Despite tuning the learning rate, the layer size, and the number of layers, this network architecture returned a constant output regardless of the input. This led us to instead implement the network without any convolutional layers.

We decided to include as input both the 2D photoelectron spectrum and the 1D X-ray spectrum based on qualitative observation. A model that contained only the 2D photoelectron spectrum as input would return an X-ray temporal field even when the input was all zeros, while the model also inputting the 1D X-ray spectrum returns only noise for a zero input, see Fig. 4.

## 4 Experimental Results and Analysis

### 4.1 Denoise with DnCNN

DnCNN improves the background level of the 2D photoelectron spectrums. However, qualitatively, the DnCNN model misidentifies some noise as signal and there are edge artifacts present (Fig. 5. It appears the denoiser has difficultly only removing background when signal and noise on the same pixel.

Comparing with the standard background subtraction method, the standard method has one group of good performance and one group of poor performance (Fig. 6). The standard method outperforms DnCNN when there is sufficient signal on the detector

### 4.2 Reconstruction with a NN

For comparison, we perform the standard MAP procedure where the L2 norm between the 2D spectrum and the reconstruction by the image formation model and a regularizer are minimized. Here we use a constraint on the fourier

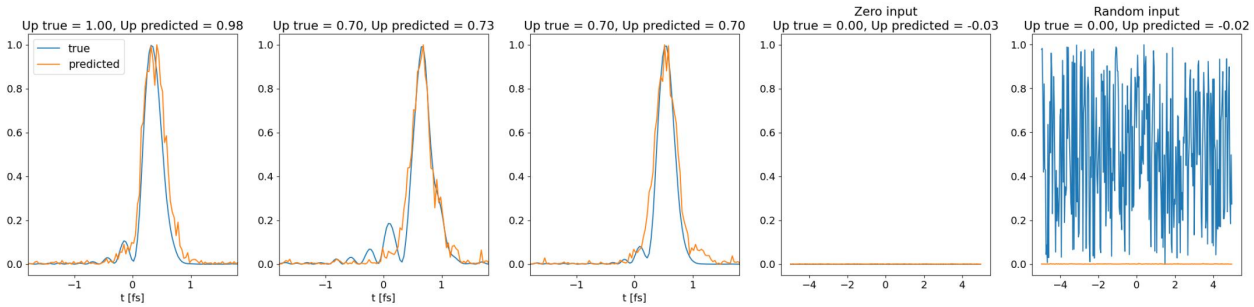


Fig. 4. Output for three members of the test set, for input of zero, and for a random input.

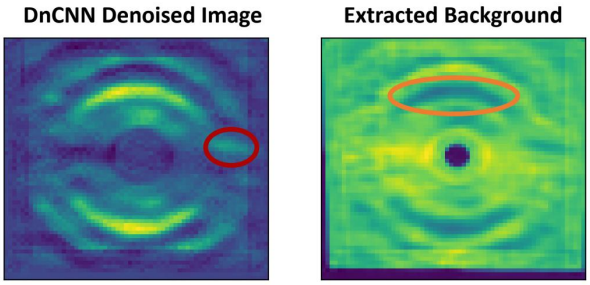


Fig. 5. DnCNN denoising errors. Noise misidentified as signal is circled in red on the left. On the right, the orange circle shows an area where background has not been identified.

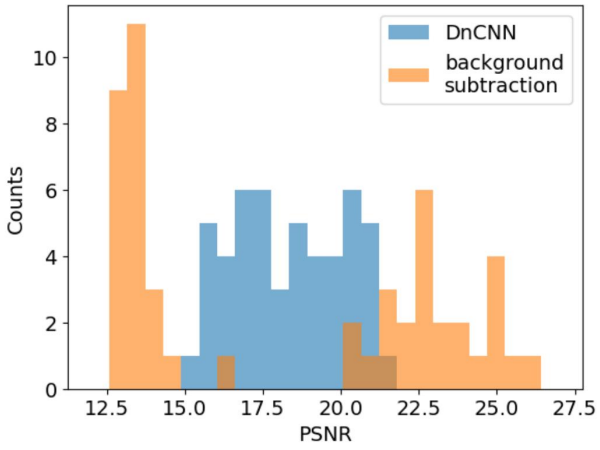


Fig. 6. PSNR of the denoised photoelectron spectra for the DnCNN method and the standard background subtraction method.

transform of the reconstructed temporal X-ray field (the spectral field) in place of a regularizer.

The NN performs poorly at reconstructing the X-ray temporal fields. Comparing the SSE for the X-ray temporal intensity profiles reconstructed by the NN and by the standard MAP method (Fig. 8), the reconstructions from the NN are less accurate with $\sim$ 5x error as the standard method reconstruction.

However, we note the NN does accurately predict the unknown variable, Up, across the whole range of Up values (Fig. 9). Even when the NN is trained only on Up values 0 to 1.0 separated by 0.1, it is able to continuously predict Up values 0 to 1.0.

## 5 Discussion

### 5.1 Denoise with DnCNN

The DnCNN denoiser does not outperform the standard background subtraction method. It may be of interest to further investigate the two populations of data found in noise removal study, particularly that which has higher PSNR with standard background subtraction than the DnCNN result . This can be used to pick a more specific training set for DnCNN.

### 5.2 Reconstruction with a NN

Currently, the NN does not accurately predict the X-ray temporal field. As at the end of training the model, the loss function has stopped decreasing, this suggests that a larger training set may be necessary to improve the model's predictions. Further improvements may also be achieved by additionally increasing the NN depth and tuning the hyperparameters.

As there is a symmetry to the photoelectron spectrum, the model may also be improved by better isolating a region of interest on the detector where the signal is most meaningful/least redundant, rather than wasting nodes on zero-signal pixels.

Since the NN was able to accurately predict the unknown variable, Up, we can modify the current reconstruction pipeline. Using the NN to predict a Up, and then only

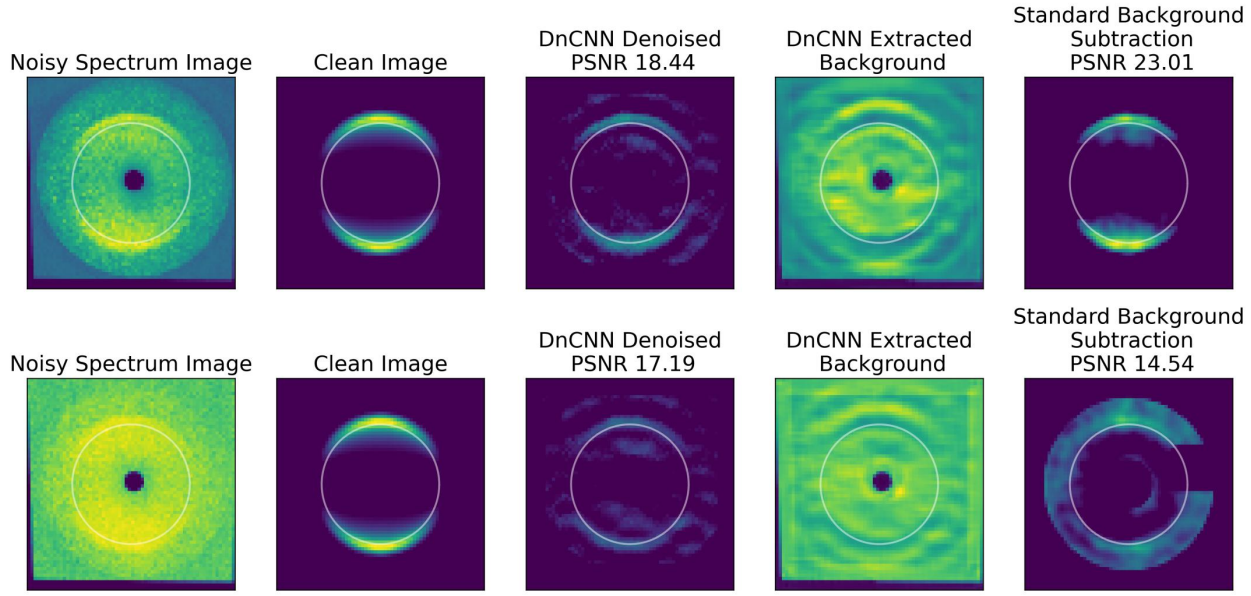


Fig. 7. Denoising with DnCNN. (Top) Denoising for a photoelectron spectrum that standard background subtraction performs well on. (Bottom) Denoising for a photoelectron spectrum that standard background subtraction performs poorly on.

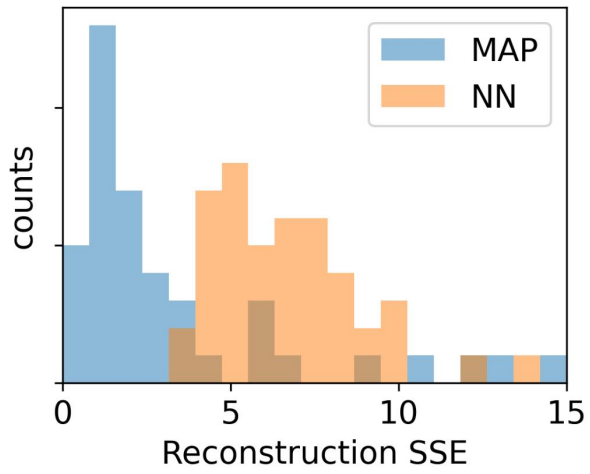


Fig. 8. SSE for the reconstructed temporal intensity profile for the standard MAP method and the NN.

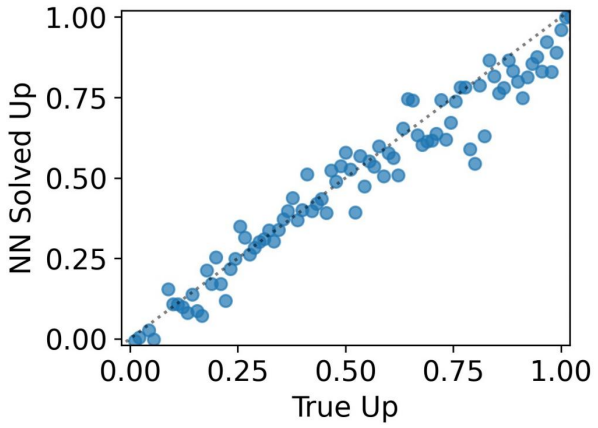


Fig. 9. Up predictions by NN for an entirely different test set than the training set (different inputs and continuous Ups)

performing MAP optimization at Up values close to this prediction rather than the whole Up range, can allow us to speed up the entire reconstruction process from 10 minutes to 3 minutes per shot.

## 6 Conclusion

Neither of the machine learning methods investigated here outperform the standards. Furthermore, for the direct reconstruction of the temporal field using the NN, the model was trained and tested on simulation data, not real experimental data. Generalizing to experimental data will likely bring further challenges. There is potential to use the Up fitting by the NN to increase the overall speed of the reconstruction pipeline, but overall, the standard method is most useful for this reconstruction problem.

## Acknowledgments

The author would like to thank Jay Shenoy for mentorship and discussion on integrating machine learning into the reconstruction pipeline.

## References

[1] S. Li, Z. Guo, R. N. Coffee, K. Hegazy, Z. Huang, A. Natan, T. Osipov, D. Ray, A. Marinelli, and J. P. Cryan, "Characterizing isolated attosecond pulses with angular streaking," *Optics Express*, 2018.

[2] J. Duris *et al.*, "Tunable isolated attosecond x-ray pulses with gigawatt peak power from a free-electron laser," *Nat. Photonics*, vol. 14, no. 1, pp. 30–36, 2020.
[3] N. Hartmann *et al.*, "Attosecond time–energy structure of x-ray free-electron laser pulses," *Nat. Photonics*, vol. 12, pp. 215–220, 2018.
[4] K. Zhang, W. Zuo, Y. Chen, D. Meng, and L. Zhang, "Beyond a gaussian denoiser: Residual learning of deep cnn for image denoising," *IEEE transactions on image processing*, vol. 26, no. 7, p. 3142–3155, 2017.
[5] A. Paszke, S. Gross, F. Massa, A. Lerer, J. Bradbury, G. Chanan, T. Killeen, Z. Lin, N. Gimelshein, L. Antiga, A. Desmaison, A. Kopf, E. Yang, Z. DeVito, M. Raison, A. Tejani, S. Chilamkurthy, B. Steiner, L. Fang, J. Bai, and S. Chintala, "PyTorch: An Imperative Style, High-Performance Deep Learning Library," in *Advances in Neural Information Processing Systems 32*, H. Wallach, H. Larochelle, A. Beygelzimer, F. d'Alché Buc, E. Fox, and R. Garnett, Eds. Curran Associates, Inc., 2019, pp. 8024–8035. [Online]. Available: http://papers.neurips.cc/paper/9015-pytorch-an-imperative-style-high-performance-deep-learning-library.pdf